HHS Public Access

Author manuscript

*Cancer Res*. Author manuscript; available in PMC 2019 January 01.

Published in final edited form as:

*Cancer Res*. 2018 January 01; 78(1): 168–181. doi:10.1158/0008-5472.CAN-17-0836.

# YAP1 and COX2 coordinately regulate urothelial cancer stem-like cells

**Akira Ooki**[1], **Maria Del Carmen Rodriguez Pena**[2], **Luigi Marchionni**[3], **Wikum Dinalankara**[3], **Asma Begum**[4], **Noah M. Hahn**[3,4,5], **Christopher J. VandenBussche**[2], **Zeshaan A. Rasheed**[4], **Shifeng Mao**[6], **George J. Netto**[2,3,5], **David Sidransky**[1], and **Mohammad O. Hoque**[1,3,5,*]

[1]Department of Otolaryngology-Head and Neck Surgery, Johns Hopkins University School of Medicine, Baltimore, Maryland 21231, USA

[2]Department of Pathology, Johns Hopkins University School of Medicine, Baltimore, Maryland 21231-2410, USA

[3]Department of Oncology, Johns Hopkins University School of Medicine, Baltimore, Maryland 21231, USA

[4]The Sidney Kimmel Comprehensive Cancer, Johns Hopkins University, Baltimore, Maryland 21231, USA

[5]Department of Urology, Johns Hopkins University School of Medicine, Baltimore, Maryland 21287, USA

[6]Allegheny Health Network Cancer Institute, Pittsburgh, PA 15212, USA

## Abstract

Overcoming acquired drug resistance remains a core challenge in the clinical management of human cancer, including in urothelial carcinoma of the bladder (UCB). Cancer stem-like cells (CSC) have been implicated in the emergence of drug resistance but mechanisms and intervention points are not completely understood. Here we report that the pro-inflammatory COX2/PGE2 pathway and the YAP1 growth regulatory pathway cooperate to recruit the stem cell factor SOX2 in expanding and sustaining the accumulation of urothelial CSC. Mechanistically, COX2/PGE2 signaling induced promoter methylation of let-7, resulting in its downregulation and subsequent SOX2 upregulation. YAP1 induced SOX2 expression more directly by binding its enhancer region. In UCB clinical specimens, positive correlations in the expression of SOX2, COX2, and YAP1 were observed, with co-expression COX2 and YAP1 particularly commonly observed. Additional investigations suggested that activation of the COX2/PGE2 and YAP1 pathways also promoted acquired resistance to EGFR inhibitors in basal-type UCB. In a mouse xenograft model of UCB, dual inhibition of COX2 and YAP1 elicited a long-lasting therapeutic response by limiting CSC expansion after chemotherapy and EGFR inhibition. Our findings provide a preclinical rationale to target these pathways concurrently with systemic chemotherapy as a strategy to improve the clinical management of UCB.

*Corresponding author as a Lead Contact: Mohammad Obaidul Hoque, DDS, Ph.D., Department of Otolaryngology and Head & Neck Surgery, The Johns Hopkins University School of Medicine 1550 Orleans Street, CRB II, 5M, Baltimore, MD 21231, Phone 410-502-8778; Fax 410-614-1411; mhoque1@jhmi.edu.

## Introduction

Urothelial carcinoma of the bladder (UCB) is the most common malignancy of the urinary tract. UCB generally follows the cancer stem cell (CSC) model, where a relatively rare population of cancer cells contributes to the driving force of tumorigenesis and metastasis due to their cancer stemness properties, including sphere formation, self-renewal, invasion and differentiation (1). CSCs are resistant to conventional chemotherapies that eliminate bulk tumor cells and they are responsible for subsequent tumor progression or recurrence, resulting in clinical treatment failure (2). Thus, the elimination of CSCs is crucial in treating malignant diseases. However, an incomplete understanding of the molecular pathways critical to CSCs has hindered the development of therapeutic strategies targeting CSCs.

Sex-determining region Y [SRY]-box 2 (SOX2) and Yes-associated protein1 (YAP1) have been studied for their possible association with CSC traits. SOX2 is a prominent transcription factor that promotes pluripotency and self-renewal in embryonic stem cells and generates induced pluripotent stem cells (iPSCs) (3). In skin squamous-cell carcinoma, lung cancer, esophageal cancer, and medulloblastoma, SOX2 plays a crucial role in maintaining CSCs and establishes a continuum between tumor initiation and progression via the direct regulation of the genes that control cancer stemness, survival, proliferation, and invasion (4–6). YAP1 is a downstream transcription coactivator of the Hippo signaling pathway and regulates the transcriptional enhancer activator domain (TEAD) transcription factors that control cell proliferation and stem cell biology (7). Moreover, the expression of YAP1 in the context of SOX2, OCT4, and KLF4 expression promotes iPSC reprogramming, indicating that YAP1 is a key regulator for the stem cell pluripotency (8). Similarly, YAP1 confers CSC traits (7) and plays a protective role against chemotherapy-induced apoptosis (9). However, the contributions of SOX2 and YAP1 to urothelial CSCs and the mechanisms regulating these molecules during urothelial tumorigenesis and therapeutic resistance remain undefined.

The inflammatory enzyme cyclooxygenase 2 (COX2) is expressed in most UCBs but not in normal urothelium (10), and direct evidence in a transgenic mouse model showed that COX2 overexpression was sufficient to cause UCB (11). Furthermore, the COX2-derived prostaglandin E2 (PGE2) pathway plays a key role in tumor-promoting inflammation, a hallmark of tumor progression (12). Notably, chemotherapy-induced apoptotic cells release PGE2, which in turn promotes CSC expansion (13). However, it is unclear how COX2/PGE2 signaling induces CSC expansion and interacts with YAP1 and SOX2 in regulating CSC and therapeutic resistance.

Approximately 10–30% of non-muscle invasive UCB will progress to muscle-invasive UCB (14), which can be stratified into basal, luminal, and p53-like types based on unique molecular and clinical features (15). Basal-type UCB is an aggressive phenotype due to its enhanced urothelial CSC traits (15,16), and the epidermal growth factor receptor (EGFR) has been demonstrated as a potential therapeutic target for this type of UCB (17). However, the mechanisms underlying an acquired resistance to EGFR-targeted therapy remain elusive.

Although YAP1 and COX2 inhibitors were known to inhibit tumor growth separately (9,18), the inhibitory effect of dual blockade on tumor growth and the interplay between COX2/PGE2-SOX2 and YAP1-SOX2 axes in the maintenance of CSCs have not been studied previously. This study was designed to investigate the mechanism of CSC maintenance in UCB and to develop therapeutic strategies to eradicate CSCs. Here, we demonstrate that the COX2/PGE2-let-7 and YAP1 signaling pathways are connected with each other to induce SOX2 expression, CSC enrichment, and acquired resistance to chemotherapy. Our findings provide a strong rationale for the dual blockade of YAP1 and COX2 signaling pathways to overcome acquired UCB resistance to gemcitabine/cisplatin (GC) chemotherapy, a common standard UCB therapeutic regimen. Furthermore, we found that concurrent inhibition of EGFR, COX2, and YAP1 potentially leads to long-term therapeutic efficacy by preventing emergence of the acquired resistance pathway in basal-type UCB.

## Materials and Methods

### Cell lines and tissue samples

The BFTC 905 and BFTC 909 cell lines were obtained from the German Collection of Microorganisms and Cell Cultures (Braunschweig), and 5637, HT-1376, J82, SCaBER, RT-4, T24, and UM-UC3 cell lines were obtained from the American Type Culture Collection (ATCC). To prepare an *in vitro* arsenic model, we chronically exposed immortalized human urothelial HUC1 cells to 1 μM of arsenic trioxide, as described previously (19).

Frozen human primary UCB and the corresponding adjacent non-malignant urothelial tissue samples were obtained from the Department of Pathology, Johns Hopkins University School of Medicine (JHUSOM). Formalin-fixed paraffin-embedded tissue microarray (TMA) sections were constructed from 528 cores from 243 UCB patient treated at JHUSOM and George Washington University. Informed consent was obtained from the patients before sample collection. Approval to conduct research on human subjects was obtained from the JHUSOM institutional review boards. This study qualified for exemption under the U.S. Department of Health and Human Services policy for protection of human subjects [45 CFR 46.101(b)] in accordance with U.S. Common Rule.

### Human Stem Cell RT$^2$ Profile PCR Array

Gene expression profiling using the Human Stem Cell RT$^2$ Profiler PCR Array (SA Biosciences) was conducted on BFTC 905 and BFTC 909 cells, HUC1 cells exposed at different periods to arsenic (6, 8, 10, and 12 months), passage-matched unexposed (UE) cells, and arsenic-exposed HUC1 cells without arsenic for 2.5 months (As+2.5M UE).

### Gene expression profiling

Expression profiles of BFTC 905 cells and arsenic-induced malignant transformed HUC1 cells were performed using the Human HT-12 v4 Expression BeadChip (Illumina). All statistical analyses were performed using the lumi and limma package in the R software (Bioconductor). The gene expression data are deposited in the NCBI Gene Expression Omnibus (GEO) database under accession ID GSE90023.

### Western blotting analysis

Whole cell lysates were extracted using the RIPA buffer (Thermo Scientific) supplemented with 10 μL/mL of the Halt™ Protease Inhibitor Cocktail Kit (Life Technologies) and 30 μL/mL of the Halt™ Phosphatase Inhibitor Cocktail Kit (Life Technologies).

### Enzyme-Linked Immunosorbent Assay (ELISA)

The PGE2 level in cell culture supernatants after CDDP treatment for 72 h was measured using quantitative ELISA kits (R&D Systems).

### Bisulfite treatment

Bisulfite treatment was conducted with an EpiTect Bisulfite Kit (Qiagen). For 5-Aza-2'-deoxycytidine (5-Aza-dC) treatment, cells were treated with 5 μmol/L of the 5-Aza-dC (Sigma-Aldrich), as described previously (20).

### Gene silencing and expression

SOX2 or YAP1 shRNA pGFP-C-shLenti Vector (SOX2-sh or YAP1-sh) was used for the knockdown of the gene expression (Origene). Non-effective 29-mer scrambled shRNA pGFP-C-shLenti Vector (Origene) was used as a control (SOX2- or YAP1-Ctrl). EF1A-Human-SOX2 lentivirus (SOX2-LV) for SOX2 induction, LentimiRa-GFP-has-let-7 lentivirus (let-7-LV) for let-7 induction, and YAP1 overexpressing lentivirus (YAP1-LV) for YAP1 induction were purchased from Cellomics Technology, Applied Biological Materials, and GenTarget, respectively. EF1A-vector control lentivirus, Lenti-III-mir-GFP control lentivirus, and CMV control lentivirus were used as controls, respectively. For the knockdown of COX2, COX-2 Silencer Select siRNA (Thermo Fisher Scientific) was used.

### *In vivo* xenograft assay

Mice were maintained in accordance with the American Association of Laboratory Animal Care guidelines. Patient-derived xenograft (PDX) tumor tissues (CTG1388 and CTG1061) were obtained from Champion Oncology (Maryland, USA). We established J16-1 PDX from the metastatic subcutaneous nodule of UCB patient who underwent surgery at the JHUSOM. Athymic (nu+/nu+) mice and NOD/SCID/IL2Rγ−/− (NSG) mice were obtained from Harlan Laboratories and the JHUSOM animal care facility, respectively. All experiments using mice were approved by the JHUSOM Animal Care and Use Committee, and the mice were maintained in accordance with the American Association of Laboratory Animal Care guidelines.

### Statistical analysis

In each set of data analyses, the estimate variation is indicated in each figure as a standard error of mean (SEM). The two groups were compared with the Wilcoxon–Mann–Whitney test. A comparison between the multiple groups was performed using the Kruskal–Wallis with post-hoc test (Dwass-Steel test) for non-parametrically continuous variables. Categorical variables were analyzed using Fisher's exact test. The level of statistical significance was set at $P < 0.05$. All statistical analyses were conducted using the JMP 12 software package (SAS Institute).

Detailed materials and methods are provided in the Supplemental Information.

## Results

### SOX2 is a critical oncogene linked to cancer stemness properties in UCB

UCB incidence and CSC expansion are reported to be associated with chronic inflammation caused by chemical carcinogens, including arsenic (21,22). To elucidate any relevant molecular alterations to the intimate connections between carcinogenesis, chronic inflammation, and CSCs in UCB, we performed gene expression profiling of arsenic-exposed HUC1 cells (As-cells) and unexposed cells (UE-cells) using both the stem cell-specific RT-PCR array and the HumanHT-12 v4 Expression BeadChip array. In As-cells compared with UE-cells, we found overexpression of SOX2 by analyzing the stem cell-specific RT-PCR array (Fig. 1A and Table S1), and the gene set enrichment analyses (GSEAs) from the BeadChip array showed that enriched oncogenic signatures of EGFR, YAP1, and COX2 (Fig. 1B). Indeed, SOX2 was preferentially expressed in UCB cell lines compared with HUC1 cells as determined by Q-RT-PCR (Fig. S1A), western blotting (Fig. 1C, **left panel**), and flow cytometry (Fig. S1B). Furthermore, spheroid cells overexpressed SOX2 as compared to parental cells (Fig. 1C and S1A–B). Interestingly, we found concomitantly increased expression of YAP1, COX2 and SOX2 in UCB spheroid cells; these had decreased expression in the re-differentiated cells (Fig. 1C, **right panel**).

Next, we determined the functional role of SOX2 in UCB. Lentivirus-based stable SOX2 knockdown (SOX2-sh) suppressed sphere-forming, self-renewal, migratory, and invasive abilities, while SOX2 induction (SOX2-LV) had an inverse effect (Fig. 1D and S1C–E). SOX2-sh spheroid cells lost cancer stemness properties such as invasion and chemotherapy resistance, while SOX2-LV cells showed opposite effect, when compared to the control (SOX2-Ctrl) spheroid cells (Fig. S1F–G). To examine the role of SOX2 on tumorigenesis, we performed a xenograft tumor-formation assay using SOX2-sh and SOX2-LV cells. A remarkable reduction in tumor volume was observed in mice injected with SOX2-sh cells compared with parental or SOX2-Ctrl cells, while enhanced tumorigenesis was observed in SOX2-LV cells (Fig. 1E and S1H), indicating the oncogenic role of SOX2 in UCB. Serially diluted SOX2-sh spheroid cells were subcutaneously injected into NOD/SCID mice. As expected, SOX2-sh spheroid cells showed significantly low tumor initiation ability, while SOX2-LV cells exhibited more aggressive ability in limiting dilution xenografts (Fig. 1E and S1H). Thus, SOX2 is an indispensable factor to maintain urothelial CSCs.

To characterize the association of SOX2 with cellular stemness-related molecules, we analyzed the expression of several stem cell markers and factors in SOX2-sh and SOX2-LV cells. Our findings demonstrated that SOX2 was associated with numerous stem cell-related key molecules including OCT4, NANOG, CD24, and CD133 (Fig. 1F and S2A–C). As CD24 and CD133 have been used to identify CSCs in various cancer types (23,24), we examined their correlation with SOX2-expressing CSCs. SOX2-expressing cells were mainly divided into two subpopulations ($CD24^+/CD133^+$ and $CD24^+/CD133^-$). Interestingly, we found that $CD24^+/CD133^+$ cells possessed higher cancer stemness properties and expression of COX2 and YAP1 compared with $CD24^+/CD133^-$ or un-sorted parental cells (Fig. S3A–G).

### The COX2/PGE2-let-7 axis regulates the SOX2 expression

To test the link between COX2/PGE2 and SOX2 in urothelial CSCs, we inhibited COX2 pharmacologically and genetically. Pharmacological inhibition of COX2 using celecoxib resulted in decreased SOX2 expression (Fig. 2A and S4A) and sphere formation (Fig. S4B), while the addition of PGE2 restored SOX2 expression (Fig. 2A, S4A, and S4C) and sphere formation (Fig. S4B). Although treatment with 10 μM celecoxib did not optimally reduce the SOX2 expression in HT1376 cells, a concentration-dependent reduction was noticed (Fig. S4A, **right panel**). Another COX2 inhibitor (etodolac) and a PGE2 receptor EP4-specific antagonist (ONO AE3 208) produced similar findings (Fig. S4D–E). Furthermore, genetic inhibition of COX2 resulted in similar findings (Fig. 2B). To further confirm the role of COX2/PGE2-SOX2 axis in maintaining urothelial CSCs, we induced SOX2 in COX2 knockdown cells and found that SOX2 induction restored COX2 knockdown-mediated inhibitory effects of CSC-related molecules (OCT4 and NANOG) and sphere formation (Fig. 2C).

Recently, several microRNAs (miRNAs) have attracted attention with regard to CSC maintenance (25). To understand the potential link between COX2/PGE2 signaling and the miRNA-mediated regulation of SOX2, we first tested the expression of a panel of miRNAs in BFTC 905 cells treated with the COX2 inhibitor celecoxib. COX2 inhibition upregulated several miRNAs including let-7, and the addition of PGE2 reduced these expressions (Fig. S4F). Because let-7 regulates CSC functions as a tumor-suppressive miRNA (26), we hypothesized that COX2 decreases let-7 expression during spheroid formation and the regulation of urothelial CSCs. Consistent with our hypothesis, we found that let-7 expression was significantly downregulated in spheroid cells compared with the parental cells, and the induction of let-7 occurred due to treatment with the COX2 inhibitor celecoxib (Fig. 2D).

To understand the molecular mechanism of let-7 downregulation, we first tested promoter methylation and expression of let-7 in UCB cells and found an inverse association (Fig. 2E), consistent with a previous report that promoter methylation of the *let-7* host gene is one of the regulatory mechanisms of let-7 expression (27). We then assessed whether COX2/PGE2-induced promoter methylation of *let-7* occurs during spheroid formation. Interestingly, we observed host gene promoter methylation of *let-7* host gene in spheroid and PGE2-treated cells, and demethylation of the promoter region of the *let-7* host gene after celecoxib treatment (Fig. 2F and S4G). Promoter methylation-mediated expression changes of let-7 were further confirmed by assessing the methylation and expression status of let-7 after treating with a demethylating agent (5-Aza-dC) (Fig. 2F–G and S4G). As DNA methyltransferases (DNMTs) are responsible for the induction of promoter methylation, we analyzed their expression in pharmacologically and genetically COX2-inhibited cells. Notably, the inhibition of COX2 decreased DNMT1 and 3A (Fig. S4H). These data suggest that COX2/PGE2 induced the promoter methylation of the *let-7* host gene, likely through the induction of DNMT1 and 3A during the acquisition of CSC traits.

It has been reported that let-7 negatively regulates high-mobility group AT-hook 2 (HMGA2) expression by targeting its 3' untranslated region (28,29) and HMGA2 induces SOX2 expression by directly binding to its promoter (30), indicating a let-7-HMGA2-SOX2

signaling pathway. To further understand the relationship between the COX2/PGE2-SOX2 axis and let-7 expression, let-7 was transduced in 5637 and BFTC 905 cells. Consistent with the previous reports (28–30), we observed a marked reduction of the expression of HMGA2 and SOX2 due to let-7 induction (Fig. S4I).

Finally, the forced expression of SOX2 in let-7-LV cells rescued the let-7-attenuated sphere-forming abilities and expression of CSC-related molecules (Fig. 2H), suggesting the COX2/PGE2-let7-HMGA2-SOX2 axis directly relates to urothelial CSC traits.

### YAP1 regulates the SOX2 expression in a COX2/PGE2 signaling-independent manner

To evaluate whether YAP1 also plays a crucial role in urothelial CSC traits, we established stable YAP1 knockdown (YAP1-sh) or overexpressed (YAP1-LV) cells. YAP1-LV cells exhibited a noticeable overexpression of SOX2, OCT4, and NANOG consistent with the increased sphere-forming and self-renewal abilities (Fig. 3A–B). In addition to CSC traits, YAP1 overexpression enhanced *in vivo* tumor growth (Fig. 3C). To assess the association between YAP1 and SOX2 in regulating CSC traits and tumor growth, YAP1-LV cells were stably transduced with SOX2-sh. As shown in Fig. 3D–E, the knockdown of SOX2 suppressed YAP1-induced cancer stemness properties and tumor growth, suggesting that YAP1 contributes to urothelial CSC traits and tumor growth via SOX2.

Because COX2 has been reported as a target gene of YAP1 (31), we assessed whether YAP1 regulates COX2/PGE2 signaling in UCB. Interestingly, both the forced expression and knockdown of YAP1 led to the upregulation of COX2 expression (Fig. 3A and 3F). Consistent with results of YAP1 genetic knockdown, the YAP1 inhibitor verteporfin (VP) induced the increased COX2 expression and decreased SOX2 expression in a dose-dependent manner (Fig. S5A). Of note, although we observed that COX2/PGE2 induced SOX2 expression (Fig. 2A, S4A, and S4C), COX2 activated by YAP1 inhibition could not fully recover SOX2 expression (Fig. 3F and S5A).

To understand the existence of YAP1-SOX2 axis independent of COX2/PGE2-SOX2 axis, we performed a chromatin immunoprecipitation (ChIP) assay and observed the direct binding of YAP1 to the enhancer region of the *SOX2* gene (Fig. 3G), consistent with a previous report (8). Although the inhibition of the COX2/PGE2-let-7 signaling axis also resulted in the upregulation of YAP1 expression, it could not lead to the total recovery of SOX2 expression (Fig. 2A–C, 2H, S4A, and S4D). These findings suggest that the YAP1 and COX2/PGE2 signaling pathways accelerate urothelial CSC traits via SOX2 in an independent manner under steady-state conditions. However, inhibition of either pathway leads to further activation of another pathway, although it could not restore SOX2 expression to the level of steady-state conditions.

To reveal whether the activation of another pathway would contribute to maintaining CSCs via the partial restoration of SOX2 expression (i.e., mutual compensation), both YAP1 and COX2 were inhibited in BFTC 905 and T24 cells. We found that the dual inhibition of YAP1 and COX2 resulted in dramatically reduced SOX2 expression, sphere formation, and tumor growth, compared with the inhibition of either alone (Fig. 3H–J). In rescue experiments, the induction of SOX2 restored the cancer stemness properties, attenuated by the dual inhibition

of YAP1 and COX2 (Fig. 3K–L). Thus, SOX2 regulates and maintains urothelial CSCs by COX2/PGE2 and YAP1 pathways in two ways; an independent regulatory mechanism under steady-state conditions and a mutually compensated manner when either pathway is inhibited. Therefore, it may be indispensable to concurrently target these pathways for the full eradication of CSCs.

## Mutual compensation of YAP1 and COX2 expression occurred through the negative feedback mechanisms of SOX2

Since the downregulation of COX2 and YAP1 occurred due to overexpression of SOX2, while upregulation of these molecules occurred due to knockdown of SOX2 (Fig. 2C, 2H, 3K, and 4A), we speculated that the mutual compensation of COX2 and YAP1 expression occurs through the negative feedback mechanism of SOX2 expression. To understand the feedback mechanism of SOX2 expression, we examined the correlation between PGE2 production and apoptosis in the YAP1-SOX2 axis, since it was previously reported that apoptotic tumor cells release COX2-derived PGE2 (13) and YAP1 plays a protective role against apoptosis (9). Interestingly, overexpression of SOX2 in YAP1-sh cells reduced apoptosis induced by YAP1 knockdown and subsequent PGE2 production, while knockdown of SOX2 in YAP1-LV cells showed an inverse effect (Fig. 4B–C and S5B–C). These findings suggest that the apoptosis induced by the inhibition of the YAP1-SOX2 axis is likely responsible for the production of COX2/PGE2. On the other hand, we found concurrent activation of Src and overexpression of YAP1 due to the inhibition of the COX2/PGE2-let-7-SOX2 signaling axis (Fig. 2A–C, 2H, S4A, and S4D), indicating a role for Src in regulating YAP1 expression (32). Indeed, YAP1 induced by COX2 inhibition was partially downregulated by Src inhibition (Fig. S5D), further suggesting Src-dependent YAP1 overexpression through the negative feedback of SOX2.

To confirm the link between the COX2/PGE2–let-7–SOX2 and YAP1-SOX2 axis, we first analyzed mRNA expression levels of YAP1, COX2, let-7, and SOX2 by Q-RT-PCR in human primary UCB and the corresponding adjacent non-malignant urothelial tissue samples. Tumors showed a trend toward higher SOX2, COX2, and YAP1 expression and a lower let-7 expression compared with the corresponding adjacent non-malignant urothelium (Fig. S6A), and significant linear correlations were observed (Fig. S6B). To determine the association among YAP1, COX2 and SOX2 expression at the protein level, we performed immunohistochemistry on 528 human UCB core tissues. The overexpression of YAP1, COX2, and SOX2 were 68.8%, 23.1%, and 25.9%, respectively (Fig. S6C). Consistent with our mRNA analysis, we found significant linear correlations among YAP1, COX2 and SOX2 expression (Fig. 4D). Moreover, the combinational assessment of YAP1 and COX2 expression was significantly associated with poor survival of patients, while SOX2 expression was not significantly associated with patient survival (Fig. S6D).

## YAP1 and COX2 inhibitors enhance chemotherapy efficacy

As COX2 and YAP1 expression mutually compensate each other, we hypothesized that dual inhibition of COX2 and YAP1 will increase therapeutic efficacy. To this end, we assessed the therapeutic efficacy of the dual inhibition of COX2 and YAP1 using the pharmacological inhibitors celecoxib and VP, respectively. The dual inhibition of COX2 and YAP1 reduced

the SOX2 expression compared with either inhibitor alone (Fig. 5A), which resulted in almost complete elimination of sphere formation (Fig. S4B). In the xenograft model, dual inhibition significantly suppressed the tumor growth rate, and the therapeutic efficacy was attenuated by SOX2 induction (Fig. 5B), strengthening the rationale for the concurrent inhibition of COX2/PGE2 and the YAP1 signaling axes to block the SOX2 expression.

Since cisplatin (CDDP) chemotherapy resulted in an increased sphere formation and the overexpression of YAP1, SOX2, and COX2 (Fig. 5C and S7A–B), we hypothesized that chemotherapy-induced COX2 and YAP1 signaling may promote CSC expansion via SOX2 overexpression and subsequent chemotherapy resistance. Consistent with our hypothesis, the dual inhibition of COX2 and YAP1 dramatically repressed CSC expansion and expression of SOX2 following CDDP treatment (Fig. 5C and S7B–C). The combination therapy of gemcitabine (GEM) and CDDP (GC chemotherapy) is a standard regimen for UCB treatment in clinical practice. The addition of dual inhibitors with GC chemotherapy demonstrated significantly continuous tumor regression and a reduced SOX2 expression compared with the addition of either inhibitor alone in the heterogeneous and clinically relevant PDX models, as well as cell line-derived xenograft models (Fig. 5D–E and S7D–E).

## The triple blockade of EGER, COX2, and YAP1 results in a continuous tumor response in basal-type UCB

As noted in Fig. 1B, we observed that EGFR was one of the most enriched oncogenic signatures in UCB cells. Here, we confirmed the efficacy of EGFR-targeted therapy (erlotinib) in several basal-type UCB cells, except BFTC 905 cells that harbor an *NRAS* mutation that drives erlotinib resistance (17)(Fig. S8A). However, erlotinib treatment also resulted in increased spheres formation in basal-type cells but not in non-basal type (Fig. 6A). Intriguingly, the level of SOX2 expression was decreased at 1 hour after treatment with erlotinib and then gradually and partially recovered in proportion to an increased COX2 expression in a basal-type-specific context (Fig. 6B and S8B). The addition of the COX2 inhibitor with erlotinib impaired the partial recovery of the SOX2 expression (Fig. 6B and S4A) and sphere formation (Fig. 6C), suggesting that the COX2-SOX2 axis plays a role in CSC enrichment following erlotinib treatment. Consistent with *in vitro* findings, dual inhibition of EGFR and COX2 resulted in a continuous tumor regression *in vivo* in comparison with EGFR inhibition alone (Fig. 6D). In contrast to COX2 overexpression, erlotinib treatment resulted in a continuously decreased YAP1 expression along with the reduced activation of AKT and extracellular signal-related kinase (ERK) (Fig. 6B). To confirm the regulation of YAP1 and SOX2 by EGFR signaling, we treated the cells with EGF and found increased YAP1 and SOX2 expression in treated cells (Fig. S8C). Since EGFR-mediated activation of YAP1 has been demonstrated via the mitogen-activated protein kinase (MAPK) or the phosphoinositide 3-kinase (PI3K)/AKT pathway (33,34), the relevance of MAPK or the PI3K/AKT pathway in regulating YAP1 expression was examined using the MAPK/ERK kinase (MEK) 1/2-specific inhibitor trametinib and PI3K-specific inhibitor LY294002, respectively. The inhibition of PI3K/AKT reduced the YAP1 and SOX2 expression in basal-type but not non-basal-type cells, while the inhibition of MAPK did not affect the expression of these molecules (Fig. S8D). Of note, a COX2 inhibitor was no longer able to induce the YAP1 expression because of the inhibition of the

EGFR-PI3K/AKT-YAP1 signaling pathway by erlotinib treatment (Fig. 6B). Therefore, the combined inhibition of EGFR and COX2 may be more effective in limiting CSC expansion via SOX2 than the EGFR inhibitor alone in basal-type xenograft models (Fig. 6D and S8E).

Further, to understand the mechanisms of the acquired resistance to EGFR inhibitor, we established an erlotinib resistant xenograft by treating the tumor bearing mice with erlotinib through multiple passages. Intriguingly, tumors with an acquired resistance to EGFR inhibitor exhibited the re-activated PI3K/AKT signaling and concomitantly elevated YAP1 and SOX2 levels, whereas EGFR-MAPK signaling remained suppressed by treatment with erlotinib (Fig. 6E). The YAP1-SOX2 axis, via re-activated PI3K/AKT signaling, may also be relevant to an acquired resistance to the EGFR inhibitor, as demonstrated by our findings that the resistant tumors again became sensitive to the EGFR inhibitor in combination with the YAP1 inhibitor (Fig. 6F). Moreover, the addition of COX2 inhibitor (i.e., triple blockade of YAP1, COX2, and EGFR) resulted in a significantly continuous efficacy by suppressing the compensatory mechanism (Fig. 6F). Finally, we assessed the efficacy of triple blockade as an initial treatment. As expected, this regimen showed a significantly continuous tumor regression compared with any other treatment (Fig. 6G). These findings suggested that the concurrent inhibition of EGFR, COX2, and YAP1 as an initial treatment led to long-term therapeutic efficacy by preventing the emergence of the acquired resistance pathway and has potential for treating basal-type UCB.

## Discussion

A growing body of evidence supports the position of rare CSCs at the top of a cellular hierarchy within neoplasms, resulting in tumorigenesis, metastasis, and treatment failure (2). Therefore, the identification of the mechanisms behind the generation and expansion of urothelial CSCs might pave the way for novel therapeutic strategies to improve prognosis of UCB patients. Here, we provide a rationale for targeting the COX2/PGE2 and YAP1 signaling pathways to attenuate CSCs by uncovering how COX2/PGE2 induces CSC expansion and interacts with YAP1 to maintain urothelial CSCs (Fig. 6H). Furthermore, we are reporting for the first time that YAP1 and COX2 inhibition increase the sensitivity of erlotinib in EGFR inhibitor resistant tumors.

The COX2/PGE2 pathway plays a key role in tumor-promoting inflammation (12), and the inhibition of this pathway suppresses CSC expansion (35). In addition, dysregulation of DNMTs expression is associated with human cancer progression, and COX2/PGE2 silences certain tumor suppressor genes via upregulation of DNMTs to promote tumor growth (36). We revealed that COX2/PGE2 signaling induces the promoter methylation of the *let-7* host gene via the upregulation of the DNMT 1 and 3A expression, resulting in a downregulated let-7 expression and subsequent SOX2 expression. As let-7 is a tumor suppressive miRNA that negatively regulates SOX2 by inhibiting HMGA2 (28–30) and frequently downregulated in UCB, targeting COX2/PGE2-let-7-HMGA2-SOX2 axis may reduce urothelial CSC generation and maintenance. On the other hand, activated YAP1 also induces SOX2 expression independent of COX2/PGE2 signaling in urothelial CSCs, and inhibition of either pathway further activates another pathway to maintain urothelial CSCs via the negative feedback mechanism of SOX2. Thus, the COX2/PGE2 and YAP1 signaling

pathways accelerate CSC expansion and mutually compensate to maintain CSCs; this explains why COX2 inhibition alone is insufficient in preventing recurrence in clinical studies (37) and provides a rationale for concurrently targeting these pathways.

SOX2 is an undruggable target because of lack of small molecule binding pockets (38). Furthermore, our findings suggest that SOX2-expressing cells were functionally heterogeneous, among which a $CD133^+/CD24^+$ subpopulation was associated with a poor outcome (Fig. S6D), and it possessed high CSC traits and increased expression of YAP1 and COX2 (Fig. S3). Thus, synergistic expression of YAP1 and COX2 (also $CD133^+/CD24^+$) among the SOX2-expressing cells may indicate a more aggressive tumor cell phenotype. Furthermore, induction of SOX2 could not completely recover the cancer stem cell properties attenuated by the inhibition of COX2 and YAP1 (Fig. 3K–L and 5B), raising the possibility that YAP1 and COX2/PGE2 signaling also contribute to maintaining SOX2-independent CSCs (39) and other tumorigenic pathways that are associated with aggressive tumor behavior. These findings may explain why the concomitant expression of YAP1 and COX2, but not SOX2, provided prognostic stratification. Thus, even if SOX2 targeting is possible in future, the targeting both the YAP1 and COX2/PGE2 signaling pathways is likely preferable for the full eradication of urothelial CSCs. Furthermore, our data support that GC chemotherapy combined with the COX2 and YAP1 inhibitors was sufficient for tumor shrinkage by targeting both CSCs and the bulk of cancer cells. Celecoxib and VP have been approved for the treatment of acute pain and macular degeneration, respectively, by the U.S. Food and Drug Administration, indicating that these drugs are relatively safe. Indeed, we did not observe body weight loss among the mice treated with these inhibitors compared with controls. However, the long-term use of selective COX2 inhibitors has raised concerns of an increased risk of serious cardiovascular events (40), and we demonstrated that the PGE2 receptor EP4 may be an alternative pharmacological target as a COX2 inhibitor (Fig. S7E).

The poor results of EGFR-targeted therapy in clinical trials suggest that treatment success depends on selecting appropriate patients (41), and basal-type UCB may benefit more from EGFR-targeted therapy because of its dependence on the EGFR signaling pathway (17). However, the inevitable development of drug resistance presents a critical challenge for any given targeted cancer therapy. Rapid signaling feedback loops that modulate the cellular response to growth factor inhibition have been demonstrated as a resistance mechanism (42). In the current study, we demonstrated that COX2 is triggered rapidly by apoptosis due to the EGFR inhibitor and/or by a compensatory mechanism because of the inhibition of YAP1-SOX2 axis. This compensatory regulation of COX2 may maintain and enrich CSC through partial restoration of SOX2 and subsequently lead to treatment failure.

In contrast to findings in lung cancer (43), we found that EGFR inhibition provided therapeutic efficacy in basal-type UCB expressing the drug efflux transporter ATP-binding cassette subfamily G member 2 (ABCG2). In addition to a target gene of SOX2, the EGFR-PI3K/AKT pathway is involved in the regulation of ABCG2 expression (44). Given our findings that the EGFR-PI3K/AKT pathway regulates the YAP1-SOX2 axis in basal-type UCB (Fig. S8D), EGFR inhibitor-suppressed SOX2 expression is likely to reduce ABCG2 expression and subsequently maintains therapeutic efficacy. On the other hand, we revealed that the YAP1-SOX2 axis was re-activated by PI3K/AKT signaling via another probable

oncogenic bypass when developing acquired resistance to EGFR inhibition. Therefore, the upregulation of ABCG2 due to the reactivation of SOX2 may contribute to acquired resistance. Collectively, our findings suggest that COX2/PGE2 and YAP1 signaling pathways are associated with acquired resistance to EGFR inhibitor therapy, and that triple blockade of EGFR, COX2, and YAP1 may be an attractive therapeutic option for basal-type UCB.

In summary, we demonstrate that the COX2/PGE2 and YAP1 signaling pathways converge to regulate urothelial CSCs via SOX2 and the activation of these pathways hampers the efficacy of systemic therapy by expanding CSCs. Our findings provide a rationale to target concurrently these pathways with systemic therapy as an effective therapeutic strategy for UCB.

## Supplementary Material

Refer to Web version on PubMed Central for supplementary material.

## Acknowledgments

**Financial support:** This work was funded by Flight Attendant Medical Research Institute Young Clinical Scientist Award 052401 YCSA (M.O.Hoque), Career Development award from SPORE in Cervical Cancer Grants P50 CA098252 (M.O.Hoque), Allegheny Health Network-Johns Hopkins Cancer Research Fund 80039465 (M.O.Hoque), P30CA006973 (L. Marchionni), and 1R01CA163594-01 (D. Sidransky and M.O.Hoque).

## References

1. Ho PL, Kurtova A, Chan KS. Normal and neoplastic urothelial stem cells: getting to the root of the problem. Nat Rev Urol. 2012; 9(10):583–94. [PubMed: 22890301]
2. Beck B, Blanpain C. Unravelling cancer stem cell potential. Nature reviews Cancer. 2013; 13(10): 727–38. [PubMed: 24060864]
3. Yu J, Vodyanik MA, Smuga-Otto K, Antosiewicz-Bourget J, Frane JL, Tian S, et al. Induced pluripotent stem cell lines derived from human somatic cells. Science. 2007; 318(5858):1917–20. [PubMed: 18029452]
4. Boumahdi S, Driessens G, Lapouge G, Rorive S, Nassar D, Le Mercier M, et al. SOX2 controls tumour initiation and cancer stem-cell functions in squamous-cell carcinoma. Nature. 2014; 511(7508):246–50. [PubMed: 24909994]
5. Bass AJ, Watanabe H, Mermel CH, Yu S, Perner S, Verhaak RG, et al. SOX2 is an amplified lineage-survival oncogene in lung and esophageal squamous cell carcinomas. Nat Genet. 2009; 41(11):1238–42. [PubMed: 19801978]
6. Vanner RJ, Remke M, Gallo M, Selvadurai HJ, Coutinho F, Lee L, et al. Quiescent sox2(+) cells drive hierarchical growth and relapse in sonic hedgehog subgroup medulloblastoma. Cancer cell. 2014; 26(1):33–47. [PubMed: 24954133]
7. Johnson R, Halder G. The two faces of Hippo: targeting the Hippo pathway for regenerative medicine and cancer treatment. Nat Rev Drug Discov. 2014; 13(1):63–79. [PubMed: 24336504]
8. Lian I, Kim J, Okazawa H, Zhao J, Zhao B, Yu J, et al. The role of YAP transcription coactivator in regulating stem cell self-renewal and differentiation. Genes & development. 2010; 24(11):1106–18. [PubMed: 20516196]
9. Ciamporcero E, Shen H, Ramakrishnan S, Yu Ku S, Chintala S, Shen L, et al. YAP activation protects urothelial cell carcinoma from treatment-induced DNA damage. Oncogene. 2016; 35(12): 1541–53. [PubMed: 26119935]

10. Shirahama T. Cyclooxygenase-2 expression is up-regulated in transitional cell carcinoma and its preneoplastic lesions in the human urinary bladder. Clinical cancer research: an official journal of the American Association for Cancer Research. 2000; 6(6):2424–30. [PubMed: 10873095]
11. Klein RD, Van Pelt CS, Sabichi AL, Dela Cerda J, Fischer SM, Furstenberger G, et al. Transitional cell hyperplasia and carcinomas in urinary bladders of transgenic mice with keratin 5 promoter-driven cyclooxygenase-2 overexpression. Cancer research. 2005; 65(5):1808–13. [PubMed: 15753378]
12. Wang D, Dubois RN. Eicosanoids and cancer. Nature reviews Cancer. 2010; 10(3):181–93. [PubMed: 20168319]
13. Kurtova AV, Xiao J, Mo Q, Pazhanisamy S, Krasnow R, Lerner SP, et al. Blocking PGE2-induced tumour repopulation abrogates bladder cancer chemoresistance. Nature. 2015; 517(7533):209–13. [PubMed: 25470039]
14. Knowles MA, Hurst CD. Molecular biology of bladder cancer: new insights into pathogenesis and clinical diversity. Nature reviews Cancer. 2015; 15(1):25–41. [PubMed: 25533674]
15. Choi W, Porten S, Kim S, Willis D, Plimack ER, Hoffman-Censits J, et al. Identification of distinct basal and luminal subtypes of muscle-invasive bladder cancer with different sensitivities to frontline chemotherapy. Cancer cell. 2014; 25(2):152–65. [PubMed: 24525232]
16. Damrauer JS, Hoadley KA, Chism DD, Fan C, Tiganelli CJ, Wobker SE, et al. Intrinsic subtypes of high-grade bladder cancer reflect the hallmarks of breast cancer biology. Proceedings of the National Academy of Sciences of the United States of America. 2014; 111(8):3110–5. [PubMed: 24520177]
17. Rebouissou S, Bernard-Pierrot I, de Reynies A, Lepage ML, Krucker C, Chapeaublanc E, et al. EGFR as a potential therapeutic target for a subset of muscle-invasive bladder cancers presenting a basal-like phenotype. Sci Transl Med. 2014; 6(244):244ra91.
18. Majumder M, Xin X, Liu L, Girish GV, Lala PK. Prostaglandin E2 receptor EP4 as the common target on cancer cells and macrophages to abolish angiogenesis, lymphangiogenesis, metastasis, and stem-like cell functions. Cancer Sci. 2014; 105(9):1142–51. [PubMed: 24981602]
19. Michailidi C, Hayashi M, Datta S, Sen T, Zenner K, Oladeru O, et al. Involvement of epigenetics and EMT-related miRNA in arsenic-induced neoplastic transformation and their potential clinical use. Cancer Prev Res (Phila). 2015; 8(3):208–21. [PubMed: 25586904]
20. Ooki A, Yamashita K, Kikuchi S, Sakuramoto S, Katada N, Kokubo K, et al. Potential utility of HOP homeobox gene promoter methylation as a marker of tumor aggressiveness in gastric cancer. Oncogene. 2010; 29(22):3263–75. [PubMed: 20228841]
21. Letasiova S, Medve'ova A, Sovcikova A, Dusinska M, Volkovova K, Mosoiu C, et al. Bladder cancer, a review of the environmental risk factors. Environ Health. 2012; 11(Suppl 1):S11. [PubMed: 22759493]
22. Tokar EJ, Qu W, Liu J, Liu W, Webber MM, Phang JM, et al. Arsenic-specific stem cell selection during malignant transformation. J Natl Cancer Inst. 2010; 102(9):638–49. [PubMed: 20339138]
23. Lee TK, Castilho A, Cheung VC, Tang KH, Ma S, Ng IO. CD24(+) liver tumor-initiating cells drive self-renewal and tumor initiation through STAT3-mediated NANOG regulation. Cell stem cell. 2011; 9(1):50–63. [PubMed: 21726833]
24. Ricci-Vitiani L, Lombardi DG, Pilozzi E, Biffoni M, Todaro M, Peschle C, et al. Identification and expansion of human colon-cancer-initiating cells. Nature. 2007; 445(7123):111–5. [PubMed: 17122771]
25. Chakraborty C, Chin KY, Das S. miRNA-regulated cancer stem cells: understanding the property and the role of miRNA in carcinogenesis. Tumour biology: the journal of the International Society for Oncodevelopmental Biology and Medicine. 2016; 37(10):13039–48. [PubMed: 27468722]
26. Yu F, Yao H, Zhu P, Zhang X, Pan Q, Gong C, et al. let-7 regulates self renewal and tumorigenicity of breast cancer cells. Cell. 2007; 131(6):1109–23. [PubMed: 18083101]
27. Nishi M, Eguchi-Ishimae M, Wu Z, Gao W, Iwabuki H, Kawakami S, et al. Suppression of the let-7b microRNA pathway by DNA hypermethylation in infant acute lymphoblastic leukemia with MLL gene rearrangements. Leukemia. 2013; 27(2):389–97. [PubMed: 22918121]
28. Roush S, Slack FJ. The let-7 family of microRNAs. Trends in cell biology. 2008; 18(10):505–16. [PubMed: 18774294]

29. Lee YS, Dutta A. The tumor suppressor microRNA let-7 represses the HMGA2 oncogene. Genes & development. 2007; 21(9):1025–30. [PubMed: 17437991]
30. Chien CS, Wang ML, Chu PY, Chang YL, Liu WH, Yu CC, et al. Lin28B/Let-7 Regulates Expression of Oct4 and Sox2 and Reprograms Oral Squamous Cell Carcinoma Cells to a Stem-like State. Cancer research. 2015; 75(12):2553–65. [PubMed: 25858147]
31. Guerrant W, Kota S, Troutman S, Mandati V, Fallahi M, Stemmer-Rachamimov A, et al. YAP Mediates Tumorigenesis in Neurofibromatosis Type 2 by Promoting Cell Survival and Proliferation through a COX-2-EGFR Signaling Axis. Cancer research. 2016; 76(12):3507–19. [PubMed: 27216189]
32. Taniguchi K, Wu LW, Grivennikov SI, de Jong PR, Lian I, Yu FX, et al. A gp130-Src-YAP module links inflammation to epithelial regeneration. Nature. 2015; 519(7541):57–62. [PubMed: 25731159]
33. Reddy BV, Irvine KD. Regulation of Hippo signaling by EGFR-MAPK signaling through Ajuba family proteins. Dev Cell. 2013; 24(5):459–71. [PubMed: 23484853]
34. Fan R, Kim NG, Gumbiner BM. Regulation of Hippo pathway by mitogenic growth factors via phosphoinositide 3-kinase and phosphoinositide-dependent kinase-1. Proceedings of the National Academy of Sciences of the United States of America. 2013; 110(7):2569–74. [PubMed: 23359693]
35. Moon CM, Kwon JH, Kim JS, Oh SH, Jin Lee K, Park JJ, et al. Nonsteroidal anti-inflammatory drugs suppress cancer stem cells via inhibiting PTGS2 (cyclooxygenase 2) and NOTCH/HES1 and activating PPARG in colorectal cancer. Int J Cancer. 2014; 134(3):519–29. [PubMed: 23852449]
36. Xia D, Wang D, Kim SH, Katoh H, DuBois RN. Prostaglandin E2 promotes intestinal tumor growth via DNA methylation. Nat Med. 2012; 18(2):224–6. [PubMed: 22270723]
37. Sabichi AL, Lee JJ, Grossman HB, Liu S, Richmond E, Czerniak BA, et al. A randomized controlled trial of celecoxib to prevent recurrence of nonmuscle-invasive bladder cancer. Cancer Prev Res (Phila). 2011; 4(10):1580–9. [PubMed: 21881030]
38. Stolzenburg S, Rots MG, Beltran AS, Rivenbark AG, Yuan X, Qian H, et al. Targeted silencing of the oncogenic transcription factor SOX2 in breast cancer. Nucleic acids research. 2012; 40(14): 6725–40. [PubMed: 22561374]
39. Schewe M, Franken PF, Sacchetti A, Schmitt M, Joosten R, Bottcher R, et al. Secreted Phospholipases A2 Are Intestinal Stem Cell Niche Factors with Distinct Roles in Homeostasis, Inflammation, and Cancer. Cell stem cell. 2016; 19(1):38–51. [PubMed: 27292189]
40. Solomon SD, McMurray JJ, Pfeffer MA, Wittes J, Fowler R, Finn P, et al. Cardiovascular risk associated with celecoxib in a clinical trial for colorectal adenoma prevention. N Engl J Med. 2005; 352(11):1071–80. [PubMed: 15713944]
41. Wong YN, Litwin S, Vaughn D, Cohen S, Plimack ER, Lee J, et al. Phase II trial of cetuximab with or without paclitaxel in patients with advanced urothelial tract carcinoma. Journal of clinical oncology: official journal of the American Society of Clinical Oncology. 2012; 30(28):3545–51. [PubMed: 22927525]
42. Rothenberg SM, Concannon K, Cullen S, Boulay G, Turke AB, Faber AC, et al. Inhibition of mutant EGFR in lung cancer cells triggers SOX2-FOXO6-dependent survival pathways. Elife. 2015; 4
43. Elkind NB, Szentpetery Z, Apati A, Ozvegy-Laczka C, Varady G, Ujhelly O, et al. Multidrug transporter ABCG2 prevents tumor cell death induced by the epidermal growth factor receptor inhibitor Iressa (ZD1839, Gefitinib). Cancer research. 2005; 65(5):1770–7. [PubMed: 15753373]
44. Porcelli L, Giovannetti E, Assaraf YG, Jansen G, Scheffer GL, Kathman I, et al. The EGFR pathway regulates BCRP expression in NSCLC cells: role of erlotinib. Current drug targets. 2014; 15(14):1322–30. [PubMed: 25479544]

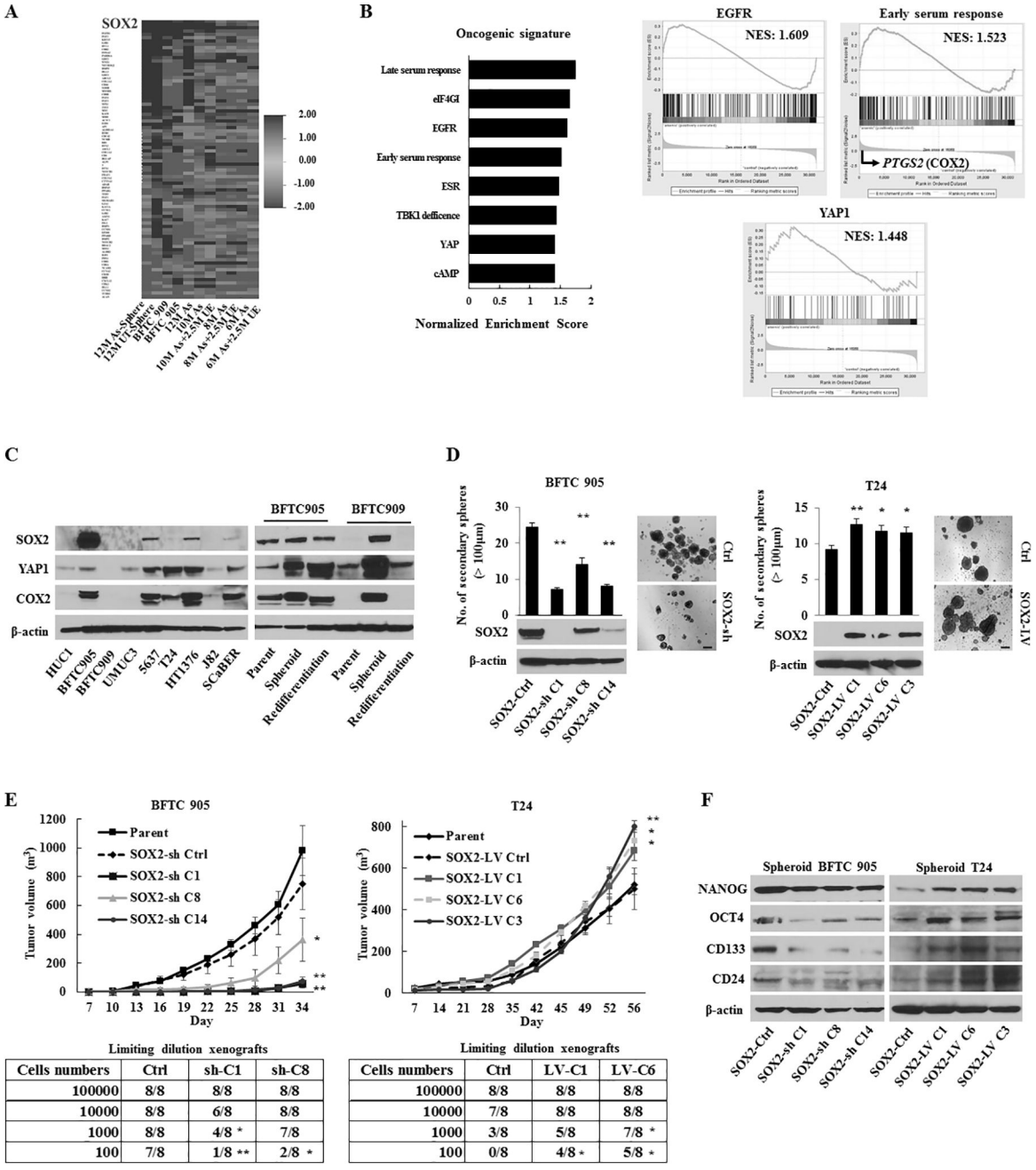


Limiting dilution xenografts

| Cells numbers | Ctrl | sh-C1 | sh-C8 |
|---|---|---|---|
| 100000 | 8/8 | 8/8 | 8/8 |
| 10000 | 8/8 | 6/8 | 8/8 |
| 1000 | 8/8 | 4/8 * | 7/8 |
| 100 | 7/8 | 1/8 ** | 2/8 * |

Limiting dilution xenografts

| Cells numbers | Ctrl | LV-C1 | LV-C6 |
|---|---|---|---|
| 100000 | 8/8 | 8/8 | 8/8 |
| 10000 | 7/8 | 8/8 | 8/8 |
| 1000 | 3/8 | 5/8 | 7/8 * |
| 100 | 0/8 | 4/8 * | 5/8 * |

**Figure 1.**

The role of SOX2 in urothelial CSC generation and maintenance. (**A**) Heat map of the relative expression using a stem cell-specific RT-PCR array in UCB cells (BFTC 905 and BFTC 909) and HUC1 cells exposed at different periods to arsenic (As cells) compared with parental HUC1 cells and the corresponding passage-matched unexposed HUC1 (UE) cells, respectively. 12M-, 10M-, 8M-, and 6M-As cells, HUC1 cells exposed chronically to arsenic for 12, 10, 8, and 6 months, respectively; 10M As+2.5M UE cells, 10M As-cells cultured for 2.5 months without arsenic to determine the arsenic withdrawal effect. (**B**) Gene set enrichment analysis (GSEA) related to the oncogenic signatures of BFTC 905 cells and As-

cells compared with UE-cells. Left, enhanced oncogenic pathways determined by a normalized enrichment score (NES); Right, the enrichment of EGFR, YAP1, and the early serum response (ESR) gene signature. *PTGS2* (encoding COX2) was the top rank of metric scores within the leading edge in the ESR signature. (**C**) Expression levels of SOX2, YAP1, and COX2 in parental and spheroid UCB cells measured by western blotting. (**D**) Number of the secondary spheres over 100 μm (left upper), representative images of sphere formation (right; scale bars, 200 μm), and western blotting of the SOX2 expression (left lower) in stable SOX2 knockdown (SOX2-sh) or SOX2 induction (SOX2-LV) cells. (**E**) *In vivo* tumorigenicity of stable BFTC 905 SOX2-sh cells (left) and T24 SOX2-LV cells (right). Upper, tumor growth curve after xenotransplantation (four mice per group); Lower, tumor initiation frequency of serially diluted BFTC 905 spheroid cells and T24 cells. (**F**) Expression levels of NANOG, OCT4, CD133, and CD24 in BFTC905 SOX2-sh and T24 SOX2-LV spheroid cells measured by western blotting.

Error bars indicate mean ± SEM. *, $P<0.05$; **, $P<0.01$ (Wilcoxon–Mann–Whitney test [**D** and upper of **E**], Fisher's exact test [lower of **E**]). See also Fig. S1–S3.

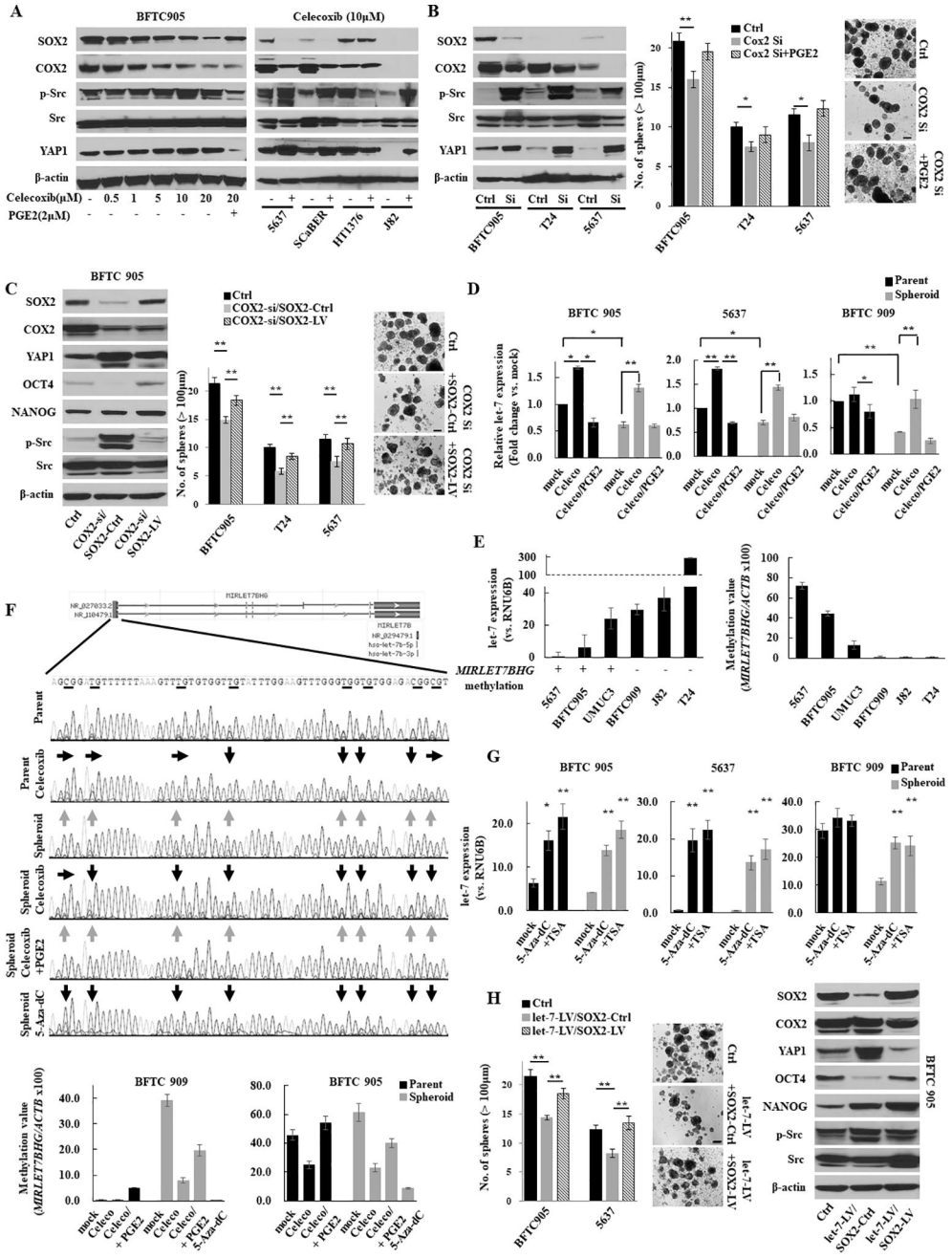


**Figure 2.**

The COX2/PGE2-let-7-SOX2 signaling axis in urothelial CSCs. (**A**) Left, western blotting after celecoxib treatment for 72 h ± PGE2 for the last 24 h in BFTC 905 cells. Right, western blotting after treatment with 10 μM of celecoxib for 72 h in UCB cells. (**B**) Left, western blot of indicated molecules after blockade of COX2 by siRNA; Middle, sphere formation assay; Right, representative images of sphere formation (scale bars, 200 μm). Data are from three independent experiments. (**C**) Western blotting analysis (left), sphere formation assay (middle), and representative images of sphere formation (right) after COX2 knockdown in SOX2-LV or SOX2-Ctrl (COX2-si/SOX2-Ctrl and COX2-si/SOX2-LV) cells.

(**D**) Expression level of let-7 in several parental or spheroid UCB cells. Expression levels of let-7 after treatment with 10 μM of celecoxib for 72 h ± 2 μM of PGE2 for 24 h were measured by Q-RT-PCR. (**E**) The expression level of let-7 and the methylation status of the let-7 host gene *MIRLET7BHG* promoter determined by bisulfite sequencing (left) and Q-MSP (right). The relative level of methylated DNA for *MIRLET7BHG* gene in each sample was determined as a ratio of the Q-MSP value of the amplified gene to *ACTB* gene, multiplied by 100. An inverse relationship between promoter methylation of the let-7 host gene and the let-7 expression was observed. (**F**) The methylation status of the *MIIRLET7BHG* promoter after treatment with 10 μM of celecoxib, 2 μM of PGE2, or 5 μM of 5-Aza-dC for 5 days in BFTC 909 cells. Upper, schematic diagram of CpG islands (red square) in the 5'-flanking region of the *MIRLET7BHG* promoter; Middle, chromatogram of the methylation status in the dinucleotide CpG within the promoter region determined by bisulfite sequencing. Gray and black arrows indicate methylated and demethylated dinucleotide CpGs within the promoter region, respectively. Lower, Q-MSP analysis. (**G**) Reactivation of let-7 after treatment with 5-Aza-dC ± Trichostatin A (TSA). The 5-Aza-dC led to the restoration of the let-7 expression. In addition, combined treatment with 5-Aza-dC and TSA upregulated the expression greater than treatment with 5-Aza-dC alone, indicating histone deacetylation may also be included in the regulatory mechanism. (**H**) Sphere formation assay (left), representative images of sphere formation (middle), and western blotting (right) after the dual induction of let-7-LV and SOX2-LV (let-7-LV/SOX2-LV). Each error bar indicates mean ± SEM. *, $P<0.05$; **, $P<0.01$ (Wilcoxon–Mann–Whitney test [**G**] and Kruskal–Wallis with post-hoc test [**B**, **C**, **D**, and **H**]). See also Fig. S4.

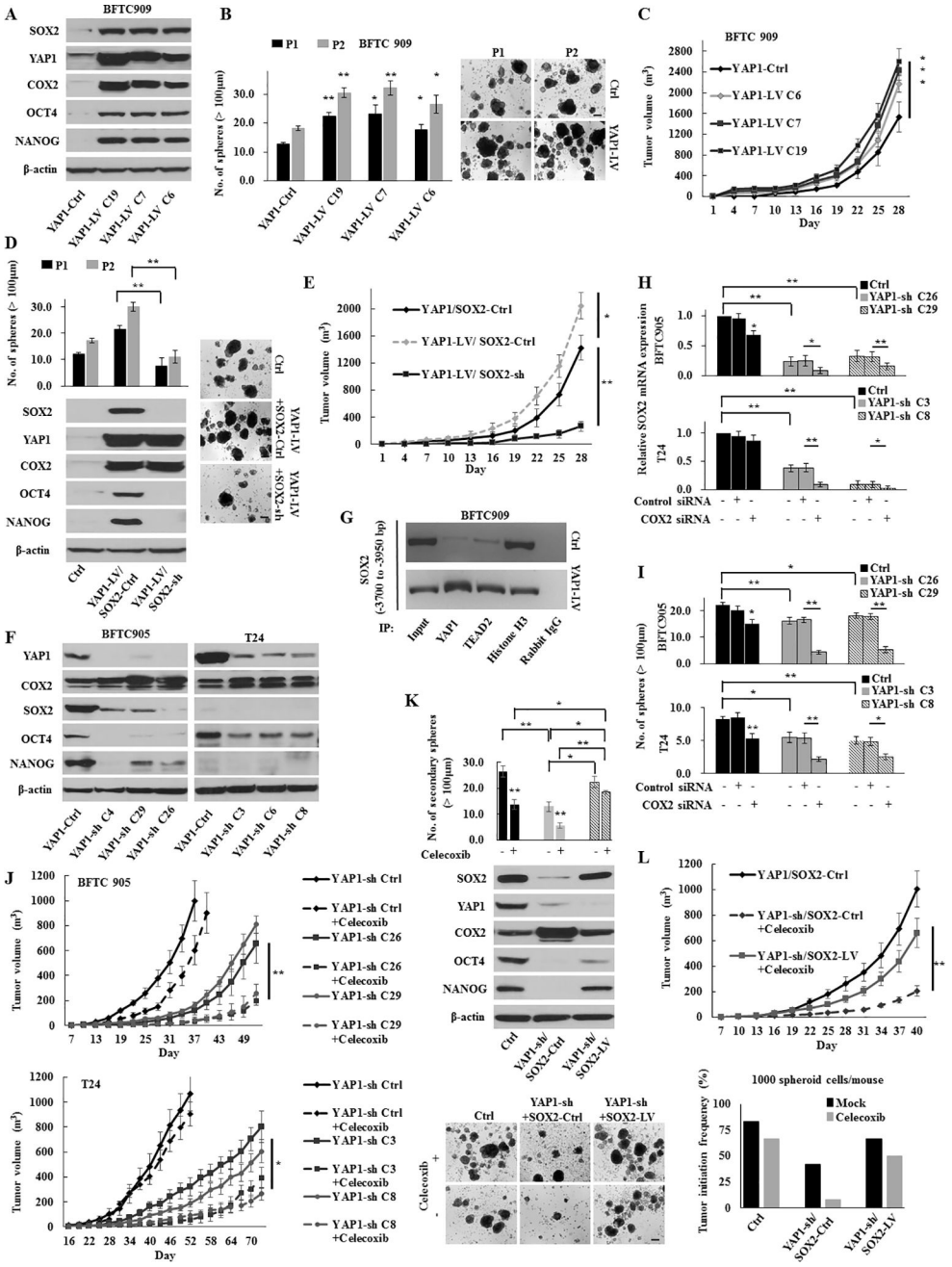


**Figure 3.**

The YAP1-SOX2 signaling axis in urothelial CSCs. (**A**) Western blotting in stable BFTC 909 YAP1-induction (YAP1-LV) cells. YAP1 induction increased the expression of SOX2 and COX2. (**B**) Sphere formation and self-renewal assays through the second (P2) passage from the first passage (P1) in YAP1-LV cells. Representative images of sphere formation (scale bars, 200 μm) were shown. (**C**) *In vivo* tumorigenesis of stable YAP1-LV cells (four mice per group). (**D**) Sphere formation and self-renewal assays (left upper) and western blotting (left lower) in BFTC 909 YAP1-LV or YAP1-Ctrl cells transduced with SOX2-LV or SOX2-Ctrl (YAP1-Ctrl/SOX2-Ctrl, YAP1-LV/SOX2-sh, and YAP1-LV/SOX2-Ctrl).

Right, representative images of sphere formation (scale bars, 200 μm). (**E**) *In vivo* tumorigenic effect of SOX2 knockdown in stable BFTC 909 YAP1-LV cells (YAP1-LV/SOX2-sh). (**F**) Western blotting in YAP1 knockdown (YAP1-sh) cells. (**G**) ChIP assays conducted on the enhancer region of the *SOX2* gene using the indicated antibodies in BFTC 909 YAP1-LV or YAP1-Ctrl cells. TEAD is a main transcription factor partner for YAP1 recruitment to chromatin. Histone H3 was used as the positive control and normal rabbit IgG was used as the negative control for immunoprecipitation. (**H**) The relative expression of SOX2 72 h after transfection with COX2 siRNA in YAP1-sh cells. The dual inhibition of COX2 and YAP1 significantly repressed the SOX2 expression compared with either inhibition alone. (**I**) A sphere formation assay in YAP1-sh cells transfected with COX2 siRNA. (**J**) *In vivo* tumorigenesis of stable YAP1-sh cells in the presence or absence of celecoxib treatment (four mice per group). (**K**) Sphere formation assay (upper) and western blotting (middle) in BFTC 905 YAP1-sh or YAP1-Ctrl cells transduced with SOX2-sh or SOX2-Ctrl (YAP1-Ctrl/SOX2-Ctrl, YAP1-sh/SOX2-LV, and YAP1-sh/SOX2-Ctrl). Lower, representative images of sphere formation (scale bars, 200 μm). (**L**) *In vivo* tumorigenic and tumor initiation effects of SOX2 induction in BFTC 905 cells with the dual inhibition of YAP1 and COX2. Upper, mice injected with stable YAP1-sh/SOX2-LV cells were treated with celecoxib (five per group); Lower, tumor initiation frequency of diluted spheroid cells (1,000 cells/injection). After the injection of cells, mice were treated with mock or celecoxib (12 per group).

Each error bar indicates mean ± SEM. *, $P<0.05$; **, $P<0.01$ (Wilcoxon–Mann–Whitney test [**B, C**, and **J**] and Kruskal–Wallis with post-hoc test [**D**, **E**, **H**, **I**, **K**, and **L**]).

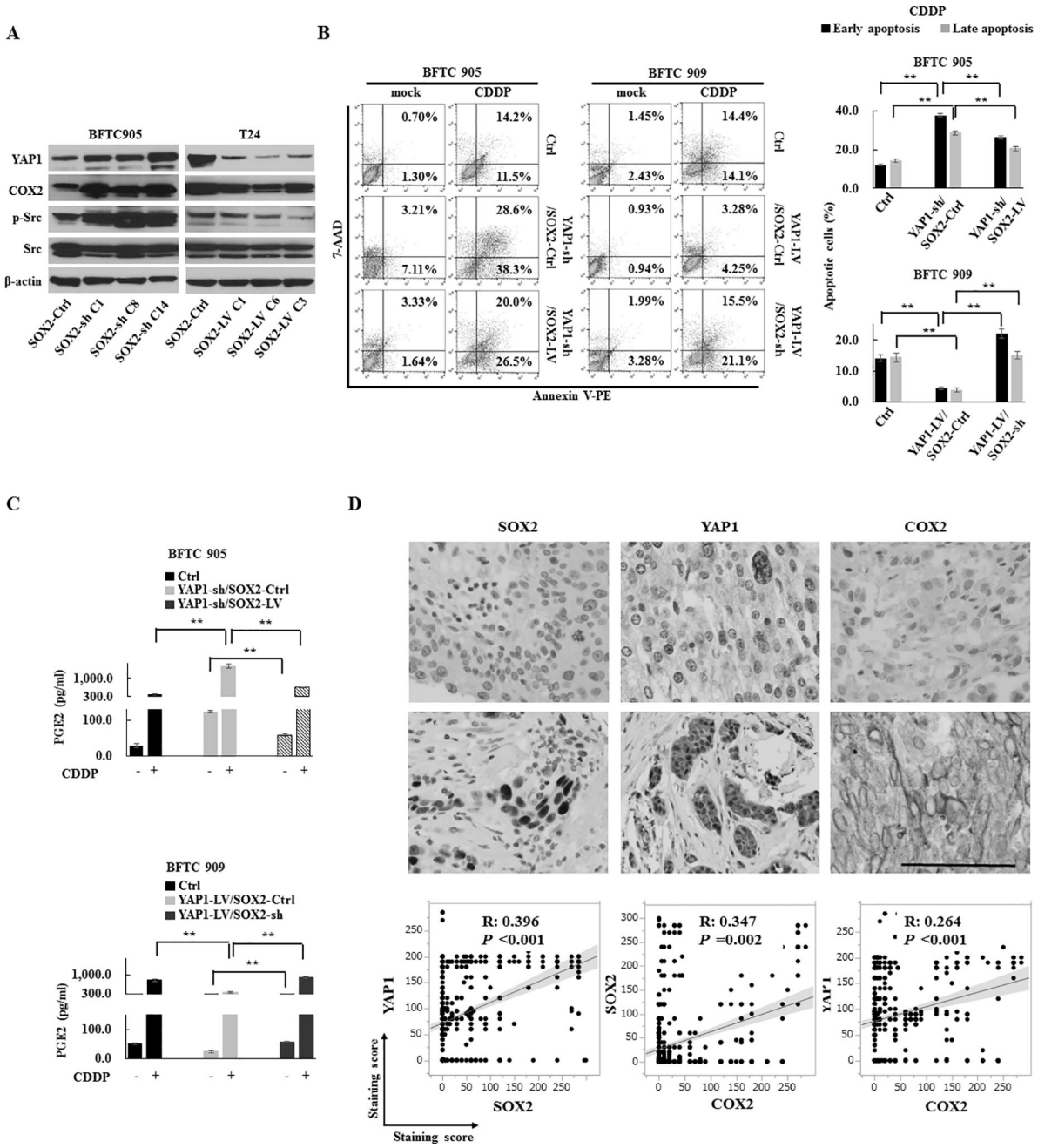


**Figure 4.**

The regulation of YAP1 and COX2/PGE2 through the negative feedback of SOX2. (**A**) The expression levels of COX2, YAP1, and p-Src in SOX2-sh or SOX2-LV cells. (**B**) Apoptosis promoted by the inhibition of the YAP1-SOX2 axis. An apoptosis assay of BFTC 905 YAP1-sh/SOX2-LV cells and BFTC 909 YAP1-LV/SOX2-sh cells treated with CDDP for 72 h. Left, representative images of early apoptosis (bottom right quadrant) and late apoptosis (top right quadrant); Right, percentage of apoptotic cells. SOX2 induction recovered the anti-apoptotic ability attenuated by YAP1 knockdown, while SOX2 knockdown attenuated the anti-apoptotic ability protected by YAP1 induction. (**C**) An ELISA assay of PGE2 after

treatment with CDDP for 72 h in YAP1-sh/SOX2-LV cells (upper) and YAP1-LV/SOX2-sh cells (lower). (**D**) The correlation among YAP1, COX2, and SOX2 in an immunohistochemistry analysis of 528 human primary UCB core tissues. Upper, representative images (scale bar, 500 μm); Lower, linear correlations among staining scores of YAP1, COX2, and SOX2.

Each error bar indicates mean ± SEM. **, $P<0.01$ (Kruskal–Wallis with post-hoc test [**B** and **C**]). See also Fig. S5 and S6.

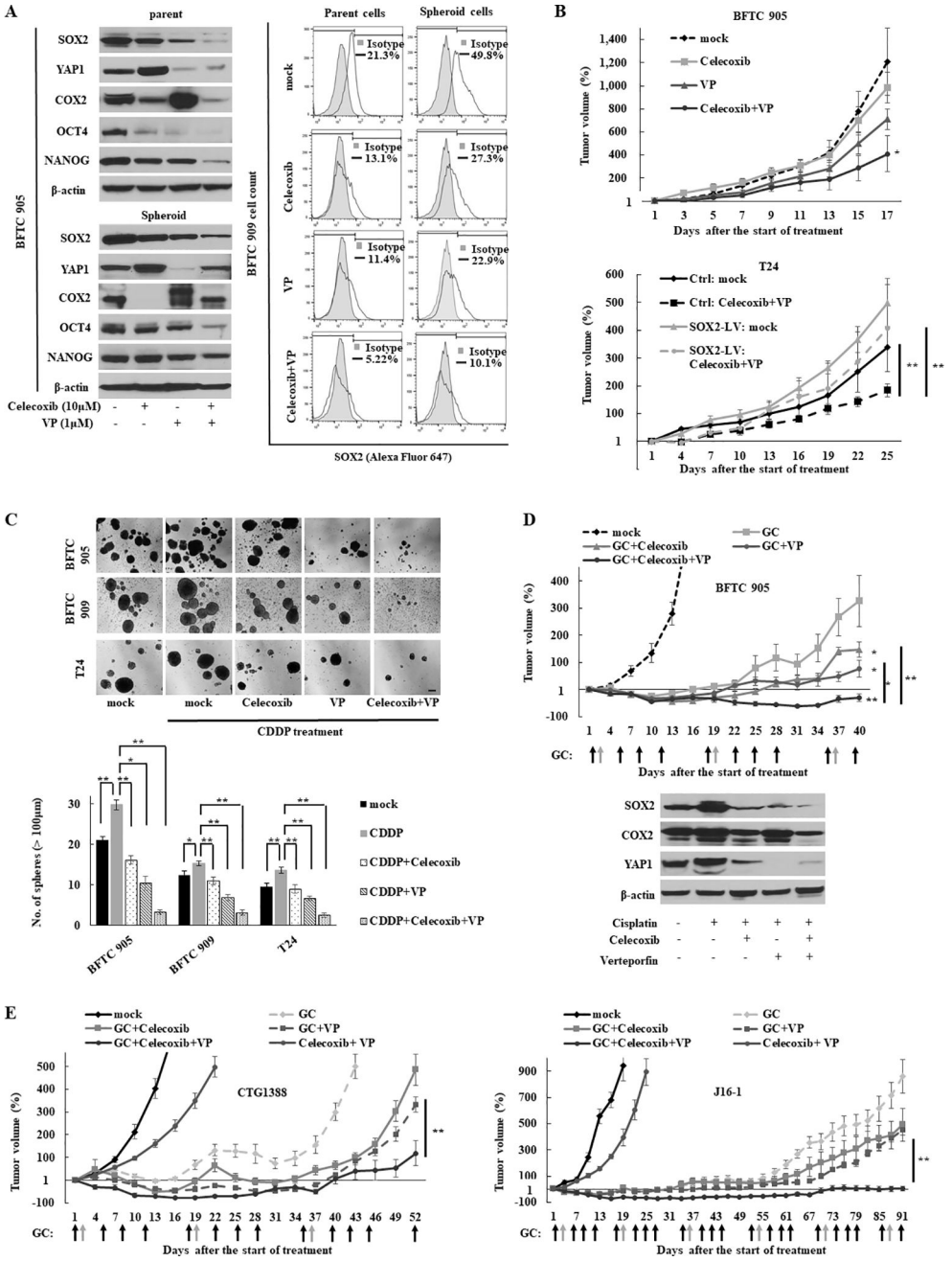


**Figure 5.**

Cancer stemness properties abrogated by the combination of the YAP1 and COX2 inhibitors. (**A**) The expression level of SOX2 after the combination treatment for 72 h, as measured by western blotting in BFTC 905 cells (left) and flow cytometry in BFTC 909 cells (right). Cells were treated with 1 μM of verteporfin (VP) and/or 10 μM of celecoxib for 72 h. (**B**) The *in vivo* therapeutic efficacy of the combination treatment in BFTC 905 (upper) and T24 SOX2-LV (lower) tumor xenografts. Growth curves were calculated by comparing the tumor size before any treatment with the size at different time points of therapy. (**C**) Sphere formation assay after cisplatin (CDDP) chemotherapy combined with VP and/or celecoxib

treatment for 72 h. Upper, representative images of sphere formation (scale bars, 200 μm); Lower, number of spheres in noted cell lines. (**D**) *In vivo* therapeutic efficacy of the combination of gemcitabine (GEM) and CDDP chemotherapy with VP and/or celecoxib (five per group). Upper, tumor growth curve. The combination therapy of GEM and CDDP (GC chemotherapy) is a standard regimen for UCB treatment in clinical practice, and the schedule of GC treatment was highlighted in black (GEM) and gray (CDDP) arrows. Growth curves were calculated by comparing the tumor size before any treatment with the size at different time points of therapy. Lower, xenograft tumor tissues were analyzed by western blotting. (**E**) The *in vivo* therapeutic efficacy of GC chemotherapy combined with VP and celecoxib in PDX models (five per group).

Each error bar indicates mean ± SEM. *, $P<0.05$; **, $P<;0.01$ (Kruskal–Wallis with post-hoc test). See also Fig. S7.

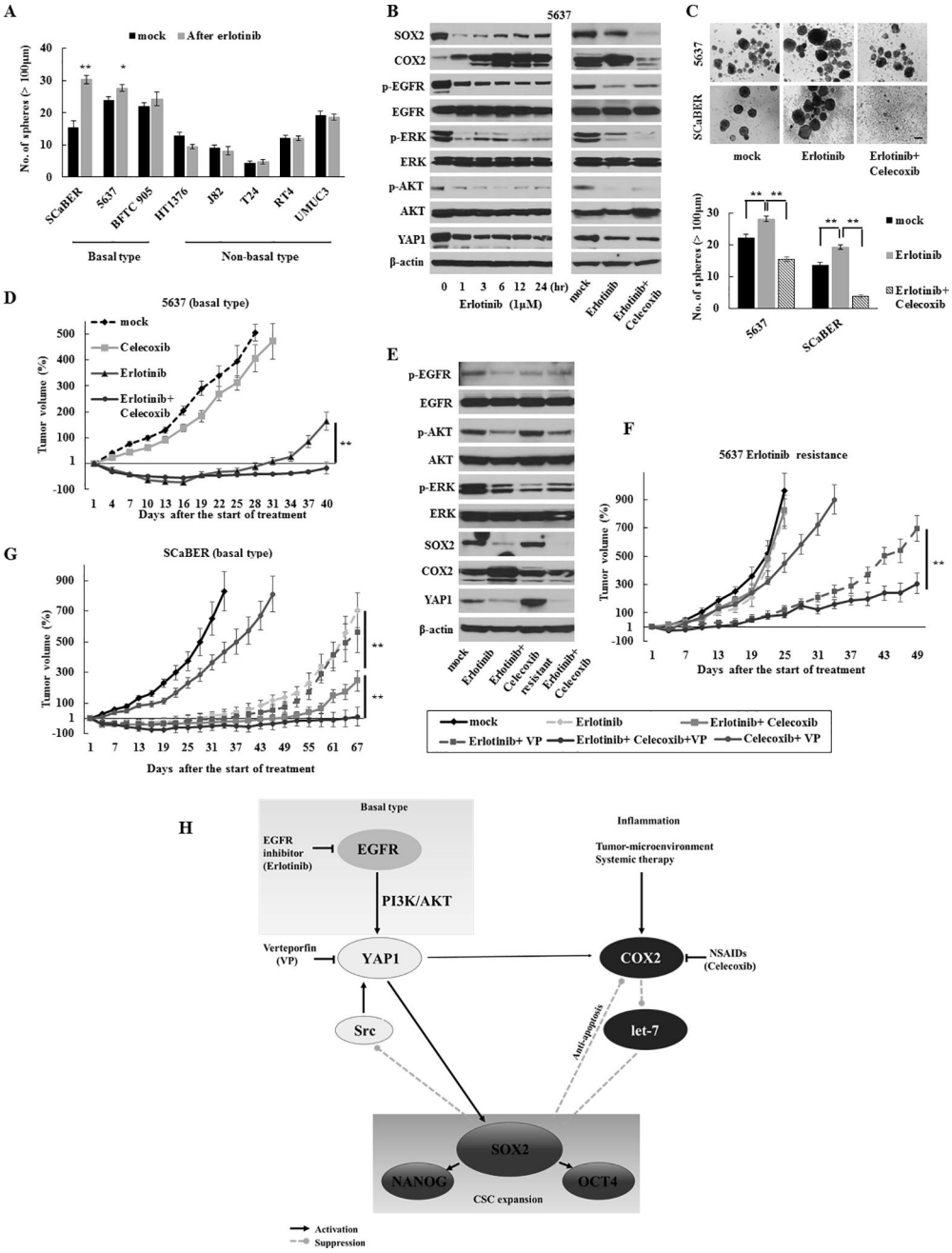


**Figure 6.**

Acquired resistance to the EGFR inhibitor due to the activation of YAP1 and COX2 signaling in basal-type UCB. (**A**) Sphere formation assay after 1 μM of erlotinib treatment for 72 h. (**B**) Dynamics of the SOX2, COX2, and YAP1 expression after treatment with 1 μM of erlotinib ± 10 μM of celecoxib in basal-type 5637 cells. Erlotinib continuously decreased the YAP1 expression and suppressed the activation of AKT and ERK. (**C**) A sphere formation assay after 1 μM of erlotinib ± 10 μM of celecoxib treatment for 72 h. Upper, representative images (scale bars, 200 μm); Lower, the number of spheres. Data are from three independent experiments. (**D**) The *in vivo* therapeutic efficacy of the dual

blockade of EGFR and COX2 in 5637 basal-type cells-derived xenograft tumors. (**E**) Western blotting in xenograft tumors that acquired resistance to erlotinib (5637 cells). Tumors resistant to erlotinib were established by consecutively passaging tumors from mice treated with erlotinib and celecoxib. (**F**) The *in vivo* therapeutic efficacy of the triple blockade of EGFR, COX2, and YAP1 in tumors with acquired resistance. (**G**) The *in vivo* therapeutic efficacy of the triple blockade of EGFR, COX2, and YAP1 as an initial treatment in ScaBER basal-type cells-derived xenograft tumors. (**H**) Schematic representation of the COX2/PGE2-let-7-SOX2 and YAP1-SOX2 axes in bladder cancer. The COX2/PGE2 and YAP1 signaling pathways are required to accelerate SOX2 and mutually compensate for each other via the negative feedback mechanism of SOX2 when either pathway was inhibited. In basal-type cells, the YAP1-SOX2 axis is regulated by the EGFR pathway via PI3K/AKT signaling but is enhanced via PI3K/AKT signaling re-activated by an oncogenic bypass following an acquired resistance to the EGFR inhibitor. NSAIDs, nonsteroidal anti-inflammatory drugs.

Each error bar indicates mean ± SEM. *, $P<0.05$; **, $P<0.01$ (Wilcoxon–Mann–Whitney test [**A** and **F**] and Kruskal–Wallis with post-hoc test [**C**, **D,** and **G**]). See also Fig. S8.